Structure and stability of fluorine-substituted benzene-argon complexes: The decisive role of exchange-repulsion and dispersion interactions

P. Tarakeshwar and Kwang S. Kim
National Creative Research Initiative Center for Superfunctional Materials, Department of Chemistry, Pohang University of Science and Technology, San 31, Hyojadong, Pohang 790-784, Korea

Elfi Kraka and Dieter Cremer
Department of Theoretical Chemistry, Göteborg University, S-41320 Göteborg, Reutersgatan 2, Sweden

(Received 11 May 2001; accepted 16 July 2001)

The van der Waals complexes benzene-argon (BAr), fluorobenzene-argon (FAr), *p*-difluorobenzene-argon (DAr) are investigated at the second-order Møller–Plesset (MP2) level of theory using the 6-31+G(*d*), cc-pVDZ, aug-cc-pVTZ, and [7*s*4*p*2*d*1*f*/4*s*3*p*1*d*/3*s*1*p*] basis sets. Geometries, binding energies, harmonic vibrational frequencies, and density distribution are calculated where basis set superposition errors are corrected with the counterpoise method. Binding energies turn out to be almost identical (MP2/[7*s*4*p*2*d*1*f*/4*s*3*p*1*d*/3*s*1*p*]: 408, 409, 408 cm^{-1}) for BAr, FAr, and DAr. Vibrationally corrected binding energies (357, 351, 364 cm^{-1}) agree well with experimental values (340, 344, and 339 cm^{-1}). Symmetry adapted perturbation theory (SAPT) is used to decompose binding energies and to examine the influence of attractive and repulsive components. Fluorine substituents lead to a contraction of the π density of the benzene ring, thus reducing the destabilizing exchange-repulsion and exchange-induction effects. At the same time, both the polarizing power and the polarizability of the π-density of the benzene derivative decreases thus reducing stabilizing induction and dispersion interactions. Stabilizing and destabilizing interactions largely cancel each other out to give comparable binding energies. The equilibrium geometry of the Ar complex is also a result of the decisive influence of exchange-repulsion and dispersive interactions. © *2001 American Institute of Physics.* [DOI: 10.1063/1.1400137]

I. INTRODUCTION

A large number of experimental and theoretical investigations in the recent past have focused on van der Waals heteroclusters consisting of rare gas atoms bound to mono- or poly-cyclic aromatic molecules,[1–6] because of their utility in understanding the structural and dynamic aspects of the solvation processes, condensed-phase properties in liquids and solids, and cluster dynamics. The experimental investigations, which have employed a wide variety of spectroscopic methods, have rendered important information on the structure, binding energies, spectral shifts, intermolecular vibrations, and ionization potentials of these rare gas complexes.[7–27] In addition, theoretical investigations, which include high-level *ab initio* calculations, have probed the structures, binding energies, and intermolecular vibrational frequencies of these complexes.[28–36] However, none of these theoretical studies has quantitatively examined the interplay of attractive and repulsive forces governing the interactions of the inert rare gas atom and the π-electron system of an aromatic or olefinic molecule.

There have been qualitative attempts to describe the magnitude of the various attractive and repulsive forces and their role in the formation of these complexes where these attempts have been based on the analysis of BSSE (basis set superposition error)-corrected electron difference density distributions $\rho(\mathbf{r})$.[37–39] One of the crucial factors, which impedes quantitative investigations, is the high level of theory needed to accurately describe the interaction of an inert rare gas and the diffuse π electron clouds of the benzene ring.[6] This is because the major attractive component of these interactions is predominantly dispersive in nature, which can only be adequately described at correlated levels of theory.

At this juncture, it is useful to recall that attractive forces are mainly comprised of electrostatic, dispersive, and inductive interactions, while the repulsive forces are mostly due to exchange repulsions. Each of these components has a different physical origin, magnitude, and directionality. Thus electrostatic forces result from interactions between the permanent electric multipole moments of the complex partners; induction forces result from interactions of the permanent electric multipole moment of one monomer with the electric multipole moment induced in the other monomer; dispersion forces result from the mutual polarization of the electron densities of the two interacting monomers; repulsive forces result from the Pauli exclusion principle, which prevents the electrons of one monomer from penetrating into the occupied space of the other monomer. Exchange repulsion increases with increasing overlap and is always destabilizing.

The recent experimental binding energies of a number of closely related π systems (benzene, fluorobenzene, *p*-difluorobenzene) with argon seem to indicate that the presence of electron-withdrawing substituents on the ring does not have a substantial effect on the observed magnitudes.[13,14,16–20,39] This is contrary to what was observed for the interactions of water with these π systems where the binding energy of the π bonded complexes de-

creases significantly as one progresses from benzene to *p*-difluorobenzene.[40–42] It should be noted that both electrostatic and dispersive interactions have a significant role in the binding of water with these π systems. Thus it is interesting and desirable to determine the magnitude of each of the individual interaction energy components of π-argon complexes and explain both the observed equilibrium geometries and the resulting binding energies. Given the earlier attempts of some of the authors of this study to explain the stability of π-rare gas complexes using a novel electron density analysis, we have also examined the efficacy of this analysis in explaining the stability of these π-argon complexes.[37–39]

The argon complexes of various aromatic π systems have been theoretically investigated by a number of groups in the past.[28–36] Thus Hobza and co-workers evaluated the geometries, binding energies and vibrational stretching modes of the benzene-argon, fluorobenzene-argon, *p*-difluorobenzene complexes at the second-order Møller–Plesset (MP2) level of theory using a 6-31+G(d) basis set to describe the π system and a [$7s4p2d$] basis set to describe the argon atom.[28–30,32] Their calculated binding energies and geometries were fairly close to the experimental values.[30] They, however, conjectured that the stabilization of the argon complexes of the fluorinated benzenes was possibly due to a charge transfer from the π system to argon.[30] Kraka and co-workers, however, observed that the charge transfer is more of an artifact of calculations not including BSSE corrections.[37] The benzene-argon complex was recently investigated by Koch *et al.* employing high-level *ab initio* methods.[33] These authors carried out CCSD(T) calculations (coupled cluster theory with single and double excitations and a perturbative inclusion of triple excitations) with a large basis set of QZ quality for the experimentally determined geometry of the benzene-argon complex and obtained a binding energy of 385 cm^{-1} in reasonable agreement with the experimental values[13,16] of ($D_0 = 340{,}316\ cm^{-1}$), considering that that zero point energy corrections are of the order of 50 cm^{-1} (see Sec. III). Due to a fortuitous cancellation of basis set and correlation errors, the experimental estimate of the binding energy is also close to the BSSE corrected binding energy of 394 cm^{-1} evaluated at the MP2/aug-cc-pVDZ level.[33]

The experimental binding energies of the benzene-argon complex merit special mention because of the presence of two different experimental estimates.[13,16] The earlier experimental estimate of an upper limit of ($D_0 = 340\ cm^{-1}$) for the C_6H_6-Ar complex was obtained by Krause and Neusser.[13] However, based on the infrared spectra of jet-cooled C_6H_6 and C_6D_6 cations complexed with Ar, Satink *et al.* observe that a D_0 of 316 cm^{-1} would be a more stringent upper limit for the dissociation energy of the neutral C_6D_6-Ar complex.[16] Therefore, in our comparisons of the calculated binding energies to the experimental estimates, we use both the aforementioned values.

The complexes of oxazole, isoxazole, and chlorobenzene with argon were at the focus of a series of theoretical investigations by Kraka and co-workers.[37–39] In their investigations, which were carried out using Spackman's 6-31G $\times(+sd,+sp)$ basis set to describe the π system and a $(14s10p2d1f)[7s4p2d1f]$ basis to describe the argon atom,[43–45] the rotational constants of the equilibrium geometries of these complexes were evaluated. Their studies also involved an innovative use of electron density maps to unravel the electronic factors determining the stability and the configuration of the equilibrium geometry. Thus an analysis of the Laplace concentration of the monomers enabled them to detect regions of strong contraction of negative charge and small exchange repulsion.

In this work, we will combine three different theoretical methods to analyze the complex stability of benzene-argon (BAr), fluorobenzene-argon (FAr), and *p*-difluorobenzene-argon (DAr) in terms of dispersive, inductive, and exchange repulsion forces. First, we will apply the conventional supermolecular (SM) approach to determine various complex properties, but in particular the complex stabilization energy. Then, we will decompose the latter into dispersive, inductive, and repulsive contributions employing symmetry adapted perturbation theory (SAPT).[46] Finally, we will merge the SM and SAPT results with the electron density analysis of Kraka and Cremer[37–39] to obtain a unified description of the three complexes where we will concentrate specifically on the following questions:

(1) Does theory confirm the experimental observation of almost identical complex binding energies for BAr, FAr, and DAr?
(2) How is the accuracy of calculated complex binding energies influenced by basis set size, BSSE corrections, and vibrational corrections? How do calculated geometries compare with the available experimental data?
(3) What are the dominant interaction terms determining the complex stability? Does the analysis of these terms lead to an explanation for the insensitivity of complex binding energies to F substitution?
(4) Do SAPT and the electron density analysis lead to the same, complementary, or controversial descriptions of the complex properties? Can one use the latter as a cost saving qualitative alternative for the time consuming and expensive SAPT description?
(5) How does F substitution influence the complex properties and can these electronic influences be explained within a simple model?
(6) What predictions can be made for other π-rare gas complexes on the basis of what is learned from the current investigation?

The paper is organized as follows: In the next section, we briefly describe the computational details. Then, in Sec. III, we present and discuss the results obtained from the decomposition of the binding energies of the π-argon complexes BAr, FAr, and DAr. Furthermore, we also examine the results obtained from the electron density distributions of these complexes. Finally, we compare the results obtained from both methods.

II. METHODS

In most theoretical investigations of van der Waals complexes, the interaction energy is evaluated either using the

SM variational method or the perturbational SAPT method.[46] In the SM method, the interaction energy is the difference between the energy of the complex and the energies of the isolated systems. Although the SM method is conceptually and computationally simple, it can not provide a clear picture of the interaction forces. However, the SAPT method[47] computes the interaction energy directly as a sum of the *electrostatic, exchange, dispersion, and induction* contributions, which provide a physical interpretation of the interactions between the complex monomers.

Given the aims of this study, we initially carried out conventional SM calculations to obtain the optimized geometries, binding energies, and vibrational frequencies of BAr, FAr, and DAr. SAPT calculations were then performed to decompose the binding energy of these complexes into individual interaction energy components.[48] The details of the calculations are briefly elaborated to aid the discussion of the results.

A. Supermolecular calculations

Complete geometry optimization of all the complexes investigated in this study were carried out at the MP2 level of theory using Pople's 6-31+G(d) basis[44] as well as Dunning's aug-cc-pVDZ and and aug-cc-pVTZ basis sets.[49] Vibrational frequencies were then evaluated for all the optimized structures at the MP2/aug-cc-pVDZ level. While all the electrons were explicitly included in the calculations carried out with VDZP basis sets, only the valence electrons were correlated in the MP2/aug-cc-pVTZ calculations.

The zero point vibrational energy (ZPVE) corrections were computed from the frequencies evaluated at the MP2/aug-cc-pVDZ level of theory. The BSSE corrections for the SM calculations were computed using the counterpoise (CP) method of Boys and Bernardi[50] according to the following calculational strategy. First, calculated binding energies ΔE_e^N were corrected by referencing them to BSSE-corrected monomer energies, which led to binding energies ΔE_e^B. Although this leads to an improvement of calculated values, the binding energies are still flawed by a geometry error caused by the fact that geometries also suffer from BSSEs.[37–39,51] Hence, in a second step, binding energies ΔE_e^B were recalculated for BSSE-corrected complex geometry thus yielding final binding energies ΔE_e^F, which represent the most reliable values.

The correction of complex geometries by the CP method was carried out in three steps. (i) The geometries of the π systems were initially optimized at the MP2/aug-cc-pVTZ level of theory. (ii) The binding energies of the complexes for different intermolecular separations were then obtained at the MP2 level using a $[7s4p2d1f/4s3p1d/3s1p]$ basis which is based on Spackman's 6-31G$(+sd,+sp)$ basis set[43,44] to describe the π system and the $(14s10p2d1f)[7s4p2d1f]$ basis set of Chalasiński and co-workers[45] to describe the argon atom. For this purpose, the MP2/aug-cc-pVTZ optimized geometry of the π system was frozen and the location of the Ar atom above the ring was varied. For the sake of brevity, this calculation will henceforth be denoted as MP2/$[7s4p2d1f/4s3p1d/3s1p]$. (iii) BSSE-corrected binding energies were fitted to a polynominal depending on the position of the Ar atom, and the equilibrium geometry was determined as the geometry that leads to a maximum binding energy.

All the SM calculations reported in this study were carried out using the GAUSSIAN[52] and COLOGNE2000 programs.[53]

B. Symmetry-adapted perturbation theory calculations

SAPT[47] provides a rigorous quantitative quantum mechanical description of the intermolecular forces and also enables one to identify the physically meaningful terms originating from classical theories of intermolecular forces. Unlike most other decomposition procedures, SAPT allows for a natural description of the interaction energy in the form of a sum of *electrostatic, induction, dispersion,* and *exchange* interactions. One can also examine the changes obtained by stepwise inclusion of electron correlation effects on these forces. In this study, the SAPT calculations were carried out using theoretical (obtained from SM calculations) or experimental geometries of the complexes. The SAPT interaction energy accurate to third order, $E_{\rm int}^{\rm (SAPT)}$, is given by Eq. (1)

$$E_{\rm int}^{\rm (SAPT)} = E_{\rm elst}^{(1)} + E_{\rm exch}^{(1)} + E_{\rm ind}^{(2)} + E_{\rm exch\text{-}ind}^{(2)} + E_{\rm disp}^{(2)} + E_{\rm exch\text{-}disp}^{(2)} + \delta_{\rm int}^{\rm HF}, \quad (1)$$

where $E_{\rm elst}^{(1)}$ is the electrostatic energy of the monomers with the unperturbed electron distribution, $E_{\rm exch}^{(1)}$ is their first-order valence repulsion energy due to the Pauli exclusion principle, $E_{\rm ind}^{(2)}$ stands for the second-order energy gain resulting from the induction interaction, $E_{\rm exch\text{-}ind}^{(2)}$ represents the repulsion change due to the electronic cloud deformation, $E_{\rm disp}^{(2)}$ is the second-order dispersion energy, $E_{\rm exch\text{-}disp}^{(2)}$ denotes the second-order correction for a coupling between the exchange repulsion and the dispersion interaction, and $\delta_{\rm int}^{\rm HF}$ includes the higher order induction and exchange corrections.

The SAPT interaction energy can also be represented as the sum of $E_{\rm int}^{\rm (HF)}$ and $E_{\rm int}^{\rm (corr)}$, where $E_{\rm int}^{\rm (HF)}$ is the sum of all the energy components evaluated at the Hartree–Fock level and $E_{\rm int}^{\rm (corr)}$ is the sum of all the energy components evaluated at the correlated level. Given the size of the systems investigated and the level of theory employed in this study to evaluate the various energy components, it was not feasible to evaluate the computationally demanding higher order components. Hence, one should expect a slight deviation of the total interaction energies evaluated using SAPT and SM calculations. This, however, does not affect our conclusions based on the magnitude of the individual interaction energy components, as was shown in a recent paper.[54] A detailed description of SAPT and some of its applications can be found in some recent references.[41,42,55–59]

III. RESULTS AND DISCUSSION

A. Geometries and energies

The optimization of the π-Ar complexes BAr, FAr, and DAr at the MP2/aug-cc-pVDZ level of theory yielded the structures shown in Fig. 1. An analysis of the optimized geometries shown in Fig. 1 of both the uncomplexed (π monomers) and complexed forms (π-Ar complexes) reveals that

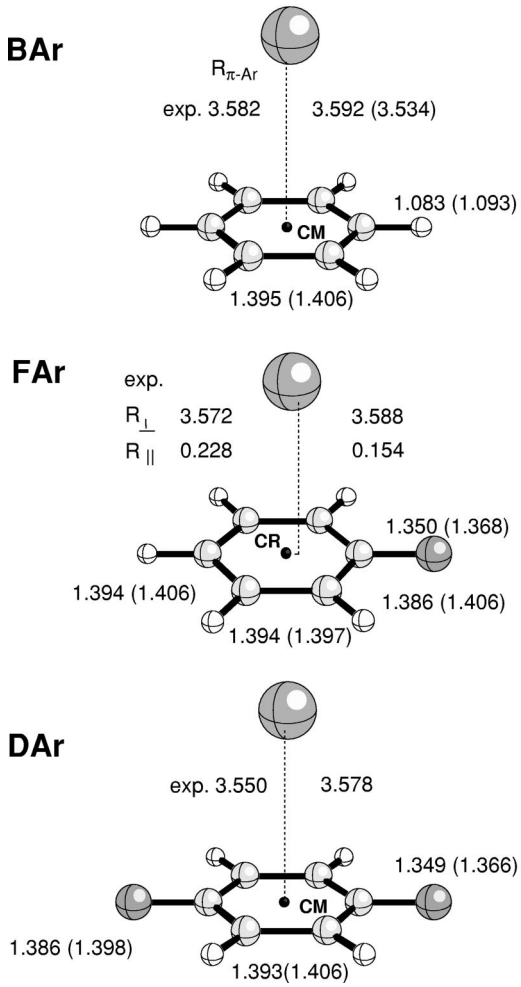

FIG. 1. MP2/aug-cc-pVTZ geometries of the benzene-Ar (BAr), fluorobenzene-Ar (FAr), and *p*-difluorobenzene-Ar (DAr) complexes. Values in parentheses correspond to MP2/aug-cc-pVDZ calculations. The position of the Ar atom was determined at the MP2/$[7s4p2d1f/4s3p1d/3s1p]$ level of theory using BSSE corrections as described in the text. CM denotes the center-of-mass for the monomer, CR the center-of-ring for fluorobenzene. Experimental (exp) values from Refs. 7, 9, and 10. All distances in Å.

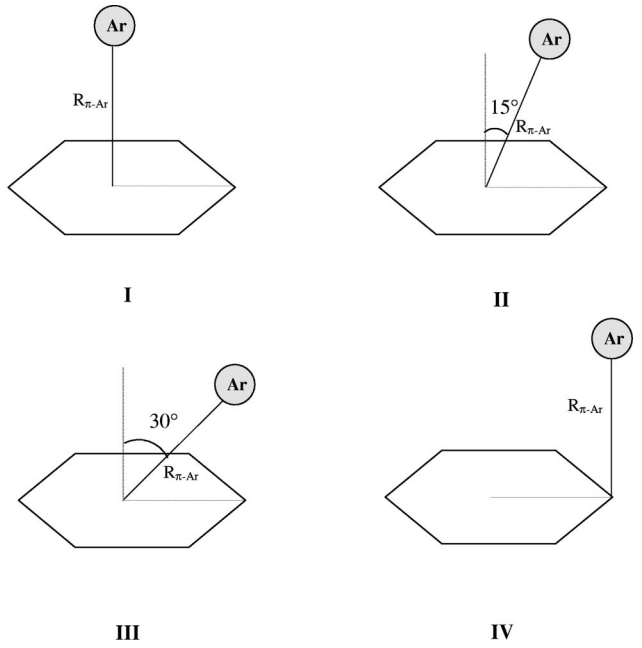

FIG. 2. Various forms of the benzene-Ar and *p*-difluorobenzene-Ar complexes, whose interaction energies are decomposed in Tables II and III. The values of $R_{\pi\text{-Ar}}$ for the BAr and DAr complexes are 3.364 and 3.335 Å at the MP2/aug-cc-pVDZ level of theory and 3.592 and 3.578 Å at the MP2/$[7s4p2d1f/4s3p1d/3s1p]$ level of theory.

there is no perceptible change in the geometries of the π system upon complex formation (changes in bond lengths: <0.001 Å; similarly small deviations from planarity). This is also evident from experiments of Weber *et al.*[7] In order to evaluate the effect of the individual interaction energy components on the observed geometries, we have also carried out calculations on the forms shown in Fig. 2.

While in the case of both the BAr and DAr complexes, the argon atom is directly located over the center of the aromatic ring, it is slightly shifted toward the C–F bond in the FAr complex. This is in line with experimental observations[8–11] and, therefore, no attempts were made to locate other plausible conformers. It can be seen from Tables I, II, and III that as one progresses from the BAr to the DAr complex, there is a gradual decrease in the intermolecular distance $R_{\pi_{\text{CM}}\text{-Ar}}$ defined as the distance between the Ar atom and the the center-of-mass of the (substituted) benzene. This decrease ranges from about 0.014 Å (MP2/$[7s4p2d1f/4s3p1d/3s1p]$), 0.03 Å (MP2/aug-cc-pVDZ), 0.018 Å (MP2/aug-cc-pVTZ) to about 0.032 Å (experimental values).[7,9,10]

The calculated intermolecular separations $R_{\pi_{\text{CM}}\text{-Ar}}$ [aug-cc-pVDZ: 3.364 (BAr); 3.335 (DAr), Table I; aug-cc-pVTZ: 3.373 (BAr); 3.355 Å (DAr), Table III] are comparatively smaller than the experimentally determined distances (BAr: 3.582; DAr: 3.550 Å).[7,9,10] This is due to the BSSE, which becomes obvious when considering BSSE-corrected geometry optimizations (Table II). Thus in case of the BAr complex, the BSSE-corrected geometry optimization at the MP2/aug-cc-pVDZ level yielded an intermolecular separation $R_{\pi_{\text{CM}}\text{-Ar}}$ of 3.534 Å and a binding energy ΔE_e^F of 399 cm^{-1}. However, the computational effort involved in determining BSSE-corrected geometries with extended basis sets for FAr and DAr is considerable and, therefore, these calculations were carried out at the MP2 level using the $[7s4p2d1f/4s3p1d/3s1p]$ basis set.

As can be seen from Table II, the intermolecular separations $R_{\pi_{\text{CM}}\text{-Ar}}$ (BAr: 3.592; DAr: 3.578 Å) obtained at this level are close to the experimental values. Moreover, a comparison of the sum of the calculated rotational constants ($A+B=2220$ MHz) of DAr with the experimentally determined sum of ($A+B=2234.6\pm2$ MHz) indicates that the calculated structure closely resembles the experimentally observed structure.[12] For FAr it is useful to give the intermolecular separation in terms of $R_{\perp}$, which is the perpendicular distance of the argon atom from the ring plane of fluorobenzene, and $R_{\parallel}$, which is the distance between the geometric center of the C_6-ring and the intersection of $R_{\perp}$ with the ring plane. Values of 3.588 and 0.154 Å were determined at the MP2/$[7s4p2d1f/4s3p1d/3s1p]$ level of theory (without BSSE-corrections at MP2/aug-cc-pVTZ: 3.364 and 0.300 Å),

TABLE I. Total binding energies and binding energy components calculated at the MP2/aug-cc-pVDZ level of theory for different forms of the benzene-, fluorobenzene-, and *p*-difluorobenzene-argon complexes.[a]

	BAr					FAr	DAr			
	I	II	III	IV	V	I	I	II	III	IV
$R_{\pi\text{-Ar}}$	3.364	3.364	3.364	3.646	3.582	3.367	3.335	3.335	3.335	3.606
A	2806	2942	3331	3097	2845	1773	1203	1464	1924	1573
B	1299	1299	1299	1145	1181	1215	1119	960	830	834
C	1299	1272	1210	1103	1181	972	733	733	733	678
ΔE_e^N	−653					−679	−698			
ΔE_e^B	−365					−353	−349			
ΔE_o	−314					−295	−305			
ΔE_{cor}	−1114					−1177	−1203			
$E_{\text{int}}^{(\text{SAPT})}$ [b]	−391	−172	731	−201	−411	−390	−394	−212	555	−273
$E_{\text{int}}^{(\text{corr})}$ [c]	−956	−1080	−1487	−811	−684	−971	−987	−1119	−1545	−847
$E_{\text{elst}}^{(1)}$	−398	−645	−1610	−441	−197	−404	−410	−626	−1434	−396
$E_{\text{exch}}^{(1)}$	1084	1709	4146	1154	542	1090	1101	1661	3836	1051
$E_{\text{ind}}^{(2)}$	−413	−1037	−3432	−822	−192	−408	−396	−920	−2633	−638
$E_{\text{disp}}^{(2)}$	−1110	−1287	−1888	−950	−770	−1120	−1133	−1307	−1923	−969
$E_{\text{exch-ind}}^{(2)}$	386	1011	3367	807	173	390	384	908	2583	633
$E_{\text{exch-disp}}^{(2)}$	112	165	348	114	59	111	111	157	312	103
$\delta_{\text{int}}^{\text{HF}}$	−52	−88	−199	−63	−25	−51	−51	−85	−186	−57

[a]All energies are in cm^{-1}; distances are in Å. See Figs. 1 and 2 for a description of the various complex forms. Form I corresponds to the MP2/aug-cc-pVDZ optimized geometry, form V to the experimental geometry. ''ΔE_e^N,'' and ''ΔE_e^B,'' represent the supermolecular binding energies without and with basis set BSSE correction, respectively. ΔE_o is the ZPVE-corrected ΔE_e^B. The frequencies for ZPVE were evaluated at the MP2/aug-cc-pVDZ level. The electron correlation energy ΔE_{cor} is the value of the $E_e(\text{MP2})$ subtracted by $E_e(\text{HF})$ at the MP2 optimized geometry. $R_{\pi_{\text{CM}}\text{-Ar}}$ is the distance from the center-of-mass of benzene, fluorobenzene, and *p*-difluorobenzene to the argon atom. A, B, C are the rotational constants in MHz.

[b]$E_{\text{int}}^{(\text{SAPT})}$ is the interaction energy of the complex form evaluated using SAPT according to Eq. (1) (see text).

[c]$E_{\text{int}}^{(\text{corr})}$ is the sum of all the energy components evaluated at the correlated level.

which indicates that BSSE corrections increase $R_\perp$ of FAr to a value between the two corresponding $R_\perp = R_{\pi_{\text{CM}}\text{-Ar}}$ values for BAr and DAr. With increasing $R_\perp$ the horizontal shift parameter $R_\parallel$ becomes smaller because the electronic effects of the F atom are less experienced by the Ar atom.

The influence of the BSSE is also reflected by the calculated binding energies (−653, −679, −698 cm^{-1}, Table I). Errors are in the range of 339–349 cm^{-1} with the complex stabilities doubled because of an unbalanced description of the monomers. They become smaller for the aug-cc-pVTZ basis (<200 cm^{-1}, Table III) in line with the well-known fact that the BSSE decreases with increasing basis set size. The BSSE-corrected SM binding energies ΔE_e^B at the MF2/aug-cc-pVDZ level (365, 353, and 349 cm^{-1}, Table I) are 40–60 cm^{-1} smaller than the corresponding energies ΔE_e^F evaluated at the MP2/[7*s*4*p*2*d*1*f*/4*s*3*p*1*d*/3*s*1*p*] level (408, 409, 408 cm^{-1}, Table II). One has to correct calculated binding energies by ZPVEs to obtain quantities ΔE_o which are directly comparable with experimental binding energies (D_0). MP2/aug-cc-pVDZ values of ΔE_o (314, 295, 305 cm^{-1}, Table I) and MP2/[7*s*4*p*2*d*1*f*/4*s*3*p*1*d*/3*s*1*p*] values (357, 351, 364 cm^{-1}, Table II) both agree reasonably with experimental values of 340 (BAr), 344 (FAr), and 339 cm^{-1} (DAr),[13,17–20] where the MP2/aug-cc-pVDZ values are 26–59 cm^{-1} too small and the MP2/[7*s*4*p*2*d*1*f*/4*s*3*p*1*d*/3*s*1*p*] values 7–25 cm^{-1} too large. If one employs the experimental estimates of 316 cm^{-1} (BAr),[16] in the comparison, the MP2/aug-cc-pVDZ values are 2–59 cm^{-1} too small and the MP2/[7*s*4*p*2*d*1*f*/4*s*3*p*1*d*/3*s*1*p*] values 7–41 cm^{-1} too large. Actually, the latter binding energies are closer to experimental values in line with the fact that this approach also gives a better account of the experimental geometries.

The binding energies obtained using VDZ basis sets in combination with the BSSE-corrected geometries are in better agreement with experimental values than those obtained with large basis sets for BSSE-uncorrected geometries. Hence, MP2/VDZ calculations, in general, but in particular the MP2/[7*s*4*p*2*d*1*f*/4*s*3*p*1*d*/3*s*1*p*] approach provide a useful description of the complex properties due to a fortuitous cancellation of basis set truncation and correlation errors, as pointed out previously by Kraka and co-workers.[37–39] Noteworthy in this connection is the fact that the most accurate estimate of the binding energy of the BAr complex obtained at the CCSD(T)/aug-cc-pVQZ level of theory yielded a value of 385 cm^{-1} corresponding to $\Delta E_o = 334\ \text{cm}^{-1}$.[33]

Although the ZPVE corrections employed in this study, i.e., 51 (BAr), 58 (FAr), 44 (DAr), were obtained using the harmonic vibrational frequencies evaluated at the MP2/aug-cc-pVDZ level, it is useful to illustrate the effect of the inclusion of both BSSE and anharmonic effects on the magnitude of the ZPVE corrections. A few studies have discussed the effect of the BSSE corrections on the calculated force constants and zero point vibrational energies.[51,60] Although the intermolecular vibrational frequencies or force constants are influenced upon optimization using BSSE corrections, the extent of the effects varies from extremely small to quite large depending on the complex and the calculational method. In the case of these weakly bound complexes, these effects are expected to be very small. Furthermore, the intermolecular stretching and bending frequencies exhibit

TABLE II. Total binding energies and binding energy components calculated at the MP2/[7s4p2d1f/4s3p1d/3s1p] level of theory for different forms of the benzene-, fluorobenzene-, and *p*-difluorobenzene-argon complexes.[a]

	BAr			FAr	DAr	
	I	IV	V	I	I	IV
$R_{\pi\text{-Ar}}$	3.592	3.853	3.582	3.607	3.578	3.830
A	2853	3104	2845	1806	1140	1495
B	1176	1051	1181	1099	1080	804
C	1176	1020	1181	898	689	641
ΔE_e^F	−408			−409	−408	
ΔE_o	−357			−351	−364	
$E_{\text{int}}^{(\text{SAPT})\text{b}}$	−420	−283	−421	−416	−416	−324
$E_{\text{int}}^{(\text{corr})\text{c}}$	−685	−579	−696	−680	−685	−582
$E_{\text{elst}}^{(1)}$	−199	−221	−206	−192	−192	−184
$E_{\text{exch}}^{(1)}$	533	577	552	510	507	479
$E_{\text{ind}}^{(2)}$	−177	−366	−184	−159	−150	−250
$E_{\text{disp}}^{(2)}$	−772	−661	−785	−759	−761	−644
$E_{\text{exch-ind}}^{(2)}$	159	355	166	150	146	249
$E_{\text{exch-disp}}^{(2)}$	59	61	60	56	55	50
$\delta_{\text{int}}^{\text{HF}}$	−23	−29	−24	−22	−21	−23

[a]All energies are in cm^{-1}; distances in Å. See Figs. 1 and 3 for a description of the various complex forms. Form I corresponds to the MP2/[7s4p2d1f/4s3p1d/3s1p] optimized geometry, form V to the experimental geometry. ΔE_e^F represents the supermolecular binding energy including BSSE corrections and being calculated at the BSSE-corrected geometry. ΔE_o is the ZPVE-corrected ΔE_e^F. Frequencies for ZPVE were evaluated at the MP2/aug-cc-pVDZ level. The electron correlation energy ΔE_{cor} is given by the difference $E_e(\text{MP2}) - E_e(\text{HF})$ calculated at the MP2 geometry. $R_{\pi_{\text{CM}}\text{-Ar}}$ is the distance from the center-of-mass of benzene, fluorobenzene, and *p*-difluorobenzene to the argon atom. A, B, C are the rotational constants in MHz.

[b]$E_{\text{int}}^{(\text{SAPT})}$ is the interaction energy of the complex form evaluated using SAPT according to Eq. (1) (see text).

[c]$E_{\text{int}}^{(\text{corr})}$ is the sum of all the energy components evaluated at the correlated level.

differing trends, with the former generally decreasing and the latter generally increasing, upon BSSE corrections. This indicates that the magnitude of the ZPVE correction is not significantly effected when the force constants are corrected for BSSE.[51]

In the case of anharmonic effects, earlier efforts to evaluate accurate ZPVE corrections inclusive of them have yielded values of 59 cm^{-1},[35] and 54 cm^{-1},[15] for the BAr complex. These values indicate that the noninclusion of anharmonic effects in the evaluation of ZPVE corrections does not significantly influence the magnitude of the calculated binding energies in these complexes. Hobza and co-workers have arrived at similar conclusions in their investigation of anharmonic effects in the more strongly bound water dimer.[60]

The MP2/[7s4p2d1f/4s3p1d/3s1p] data listed in Table II confirm that complexes BAr, FAr, and DAr possess a complex binding energy ΔE_e^B of 408±1 cm^{-1}, which is slightly varied when adding ZPVE corrections. This similarity is remarkable in view of the calculated variation in the distance $R_{\pi\text{-Ar}}$ of 0.03 Å (BSSE-corrected: 0.014 Å, Table II). As it is hardly possible that all interaction terms are insensitive to F substitution of the benzene ring, the ratio of attractive and repulsive forces in complexes BAr, FAr, and DAr must be conserved in some way, despite changes in individual interaction terms. Therefore, it has to be clarified how this balance of attractive and repulsive forces is retained for the three complexes.

Such an analysis must be based on BSSE-corrected SAPT values obtained at BSSE-corrected geometries because a comparison of the data in Tables I and II reveals that the former (calculated for BSSE-uncorrected geometries) differ considerably from the latter (calculated for BSSE-corrected geometries). The magnitude of all the interaction energy components is significantly higher in the structures optimized at the (not BSSE-corrected) MP2/aug-cc-pVDZ level of theory. Even though this increase can be readily attributed to the decreased intermolecular separation observed for these structures as a consequence of the BSSE, it can be seen that the increase observed in the attractive components is partially balanced by an equally large increase in the repulsive components.

Changes in the magnitude of electrostatic, dispersion,

TABLE III. Total binding energies and binding energy components calculated at the MP2/aug-cc-pVTZ level of theory for different forms of the benzene-, fluorobenzene-, and *p*-difluorobenzene-argon complexes.[a]

	BAr(I)	FAr(I)	DAr(I)
$R_{\pi\text{-Ar}}$	3.373	3.393	3.355
A	2853	1821	1197
B	1299	1198	1140
C	1299	969	735
ΔE_e^N	−683	−688	−696
ΔE_e^B	−501	−505	−502
ΔE_o	−450	−446	−458
ΔE_{cor}	−1210	−1200	−1220

[a]All energies are in cm^{-1}; distances are in Å. See Figs. 1 and 3 for a description of the various complex forms. The frequencies for ZPVE were evaluated at the MP2/aug-cc-pVDZ level. See footnote of Table I for other definitions.

and exchange-repulsion interaction energy components caused by the F substituent(s) also depend on how the geometry optimizations were carried out. Thus in the MP2/aug-cc-pVDZ calculations without BSSE corrections (Table I), one observes an increase in these components as one progresses from BAr to DAr, with the increase being more pronounced in the case of dispersion energies, than in the exchange-repulsion and electrostatic energies. A decrease is, however, observed in the calculations (Table II) carried out at the MP2/$[7s4p2d1f/4s3p1d/3s1p]$ level, with the decrease being more pronounced in the case of exchange-repulsion than dispersive energies. Although the trends in the net interaction energies are very similar for both calculational procedures, one notes that the noninclusion of BSSE in the geometry optimization dramatically alters the trends observed in the case of individual interaction energy components. *The altered trends can also be attributed to the different distance dependencies of the individual interaction energy components because the intermolecular separations in the BSSE-uncorrected geometries are far smaller than the corrected geometries*. Therefore, we will base the following discussion (if not otherwise noted) on energy data based on the BSSE-corrected geometries of Table II.

It can be seen from the magnitude of the total interaction energy $E_{\text{int}}^{(\text{SAPT})}$ and the sum of all the interaction energy components evaluated at the correlated level ($E_{\text{int}}^{(\text{corr})}$, Tables I and II) that all π-Ar complexes are strongly repulsive at the Hartree–Fock level of theory. However, for both the HF and correlation corrected contributions it holds that BAr, FAr, and DAr do not differ much (Table II). The magnitude of the electrostatic energies $E_{\text{elst}}^{(1)}$ (-199, -192, -192 cm^{-1}, Table II) has little effect on the relative magnitudes of total interaction energies. The major attractive force in all of these complexes is the dispersive interaction $E_{\text{disp}}^{(2)}$ (-772, -759, -761 cm^{-1}, Table II) with its contribution being nearly four times larger than that of the corresponding electrostatic interaction. The dominance of dispersive interactions in the attractive forces of π-Ar complexes BAr, FAr, and DAr is in marked contrast to the dominance of electrostatic and inductive interactions observed in the case of conventional hydrogen bonded systems. The magnitude of the repulsive contribution, which predominantly emerges from the exchange-repulsive term $E_{\text{exch}}^{(1)}$, is of particular interest for the equilibrium geometry of these complexes, an issue which will be examined in more detail when analyzing the electron density distributions of BAr, FAr, and DAr (see Sec. III B).

A fluorine substituent leads to a contraction of the π-density of the ring, which can be made visible by subtracting the $\rho(\mathbf{r})$ of benzene from $\rho(\mathbf{r})$ of *p*-difluorobenzene (see Fig. 3). If one keeps the geometry of benzene fixed to that of *p*-difluorobenzene (apart from the C–X bonds in para-position), differences in the electron density can be directly analyzed for regions far from the C–X bonds. Thus the F substituents diminish the π-density above and below the six-membered ring (dashed contour lines) and contract it toward the C atoms (solid contour lines). The σ-electron withdrawing power of the F substituents is reflected by the decrease of the electron density in the ring plane (in particular the ring center) and is actually responsible for the changes in the

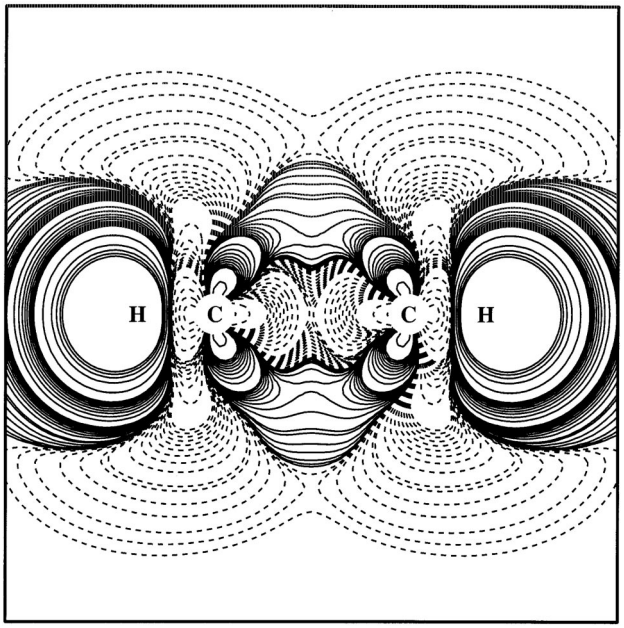

FIG. 3. Contour line diagram of the MP2 difference electron density distribution $\Delta\rho(\mathbf{r})=\rho(p\text{-difluorobenzene})-\rho(\text{benzene})$ calculated with the $[4s3p1d/3s1p]$ basis at MP2/aug-cc-pVTZ optimized geometries. Reference plane is the plane perpendicular to the benzene ring that contains the C–X bonds (X=H or F). Contour lines range from 2×10^{-6} to $2\times10^{-1}[e/\text{Bohr}^3]$. Solid lines correspond to an increase of the electron density upon change from benzene to *p*-difluorobenzene, dashed lines to a decrease.

π-space. For the complex formation, however, the most important effect of the F substituents is the reduction of the density above and below the ring plane.

The decrease in the outer π-electron density of FAr facilitates a closer approach of the argon atom because of reduced exchange-repulsion interactions (Table II). The presence of an electron-withdrawing substituent such as F also leads to a decrease in the magnitude of the induction energy $E_{\text{ind}}^{(2)}$ which can be readily attributed to the diminished π-electron density above the ring as one progresses from benzene to *p*-difluorobenzene. Since π-σ^* interactions also contribute to the induction energies, the enhanced stability of the highest occupied molecular orbitals (HOMOs) in the fluorinated benzenes also decreases the induction energy contribution in their argon complexes.

A contraction of the π-electron density in the F-substituted complexes also influences the magnitude of the dispersion energy, which becomes smaller (less stabilizing) (Table II). Although the corresponding water monomer complexes of these π systems also exhibit a similar decrease in the magnitudes of the various interaction energy components, the decrease is much more pronounced therein and is in sharp contrast to what is observed in case of the π-Ar complexes.[40,61] Thus as one progresses from benzene to *p*-difluorobenzene, the magnitude of the total binding energy of their water monomer complexes decreases by about 60%, electrostatic by about 60%, exchange-repulsion by about 40%, induction by about 40%, and dispersion by about 20%.[61]

Given the definition of exchange-repulsion,[62] its magni-

tude can be directly correlated to both the magnitude of the overlap of the filled orbitals of the π system and the argon atom (four-electron repulsion effects) and the extent of penetration of negative charge. Since the magnitude of this overlap increases exponentially with decreasing intermolecular separations, it is of interest to examine on how F substitution would influence the energetics and hence the position of the argon atom over the ring. In order to do so, we carried out calculations on forms II, III, and IV (Fig. 2) of the BAr and DAr complexes. While calculations on form IV were carried out using both the aug-cc-pVDZ and $[7s4p2d1f/4s3p1d/3s1p]$ basis sets, forms II and III were investigated using only the aug-cc-pVDZ basis set.

It can be seen from Tables I and II that a shift of the argon atom from the center of the aromatic ring (form I) to a position directly above one of the aromatic carbon atoms (form IV) leads to a decrease in the (stabilizing) dispersive energies $E^{(2)}_{\text{disp}}$ for both the BAr and DAr complexes (by 111 from -772 to -661 and by 117 from -761 to -664 cm^{-1}, Table II). The magnitude of the exchange-repulsion energy $E^{(1)}_{\text{exch}}$, however, distinguishes between the BAr and DAr complexes in the way that BAr is destabilized (by 552 $-533=44$ cm^{-1}, Table II), while DAr is stabilized (by 479 $-507=-28$ cm^{-1}) when converting the complex from I into IV. There are also changes in the electrostatic energy $E^{(1)}_{\text{elst}}$ [$-177-(-366)=-189$ cm^{-1}, Table II] and the induction energy $E^{(2)}_{\text{ind}}$ [$-150-(-250)=-100$ cm^{-1}], however, the latter is largely canceled out by an accompanying increase in the exchange-induction energy $E^{(2)}_{\text{exch-ind}}$ ($355-159=+196$ and $249-146=103$ cm^{-1}, Table II). The changes in the electrostatic energies do not compensate for the observed reduction of the stabilizing dispersive energies by 111 and 117 cm^{-1}, respectively, and, as a result, the net binding energy of form IV is lower than that of form I in both the BAr and DAr complexes [by $137=-283-(-420)$ and $92=-324-(-416)$ cm^{-1}, Table II].

Calculations on forms II and III (Table I) also distinguish between the characteristics of the BAr and DAr complexes. Thus while stabilizing dispersive interactions become larger for DAr [$-1923-(-1133)=-790$ cm^{-1}, Table I] than for BAr [$-1888-(-1110)=-778$ cm^{-1}], the increase in destabilizing exchange-repulsion is more pronounced in the case of BAr ($4146-1084=3062$ versus $3836-1101=2735$ cm^{-1}, Table I). This is parallel to the fact that exchange interactions distinguish between BAr and DAr, as discussed above for the difference $E^{(1)}_{\text{exch}}(\text{IV})-E^{(1)}_{\text{exch}}(\text{I})$.

An important point, which emerges from the above discussion, is that the magnitude of both the exchange-repulsion and dispersion interactions have a crucial role in determining the equilibrium geometry of these π-argon complexes. As the dispersive effects are maximized both by a decrease in the intermolecular separation and an increase in the number of π-electrons participating in the interaction, the decrease observed in the exchange-repulsion of DAr as one progresses from form I to form IV also explains the shifting of the argon atom toward the C–F bond in the case of FAr.

B. Electron density analysis

Changes accompanying the complex formation can also be investigated by calculating difference electron density distributions

$$\Delta\rho(\mathbf{r})=\rho(\text{complex})-\sum_i \rho_i(\text{monomer})^{\text{DCBS}}, \quad i=1,2, \tag{2}$$

where the monomer density distributions $\rho_i(\text{monomer})^{\text{DCBS}}$ are calculated in the dimer-centered basis set (DCBS) to correct for BSSE. In Fig. 4, MP2/$[7s4p2d1f/4s3p1d/3s1p]$ difference density distributions $\Delta\rho(\mathbf{r})$ determined for BAr, FAr, and DAr at their equilibrium geometries are shown with regard to a plane containing the Ar atom, the center of the benzene ring, and the C–X bonds (X=H or F) in *para*-position. An increase of the difference density due to complex formation is indicated by solid contour lines, a decrease by dashed contour lines.

Complex formation leads to an increase of the electron density distribution in regions 1 and 3, however, to a decrease in regions 2 and 4, i.e., regions of positive $\Delta\rho(\mathbf{r})$ are followed by regions of negative $\Delta\rho(\mathbf{r})$ in a regular pattern. This pattern is similar for complexes BAr, FAr, and DAr and can be explained in the following way. The Ar atom pushes π-electron density out of the intermolecular region 2 (Fig. 4) toward and through the center of the benzene ring (region 3). The benzene ring, in turn, pushes the density of the Ar atom toward its back (region 1), however, part of this density is stopped by the Ar nucleus so that a build up of electron density in a small region in front of the Ar nucleus can be observed (region 2c). Overall the calculated $\Delta\rho(\mathbf{r})$ indicates that complex formation leads to polarization of both the density at Ar and the π-density of the benzene ring. Small dipole moments are induced for both the Ar atom and the benzene ring [see Fig. 4(a)] thus creating some attractive induction forces.

The calculated difference electron density distribution $\Delta\rho(\mathbf{r})$ reflects the important role of exchange repulsion, which leads to a polarization of the charge distribution of the monomers upon complex formation. For BAr and DAr, the energetically favorable position is above the ring center because the destabilizing exchange-repulsion effects are small. In this position, the Ar atom can approach the ring closely so that stabilizing dispersion effects involving the electrons of the six C atoms become large.

Comparison of Figs. 4(a) and 4(c) shows that less electron density is pushed out of region 2 in the case of DAr. Accordingly, the polarization of the density at Ar and at the benzene ring is smaller, which can be verified by inspection of Fig. 4(b). There, the density at the Ar atom is distorted in the way that the stronger effect of the π-density associated with C4H (as compared to that associated with C1F) becomes visible [see arrows indicating polarization directions of the density in Fig. 4(b)]. While a quantification of these effects is difficult, they can be better illustrated when depicting the changes in the electron density distribution caused by a variation of complex formation due to substituent effects.

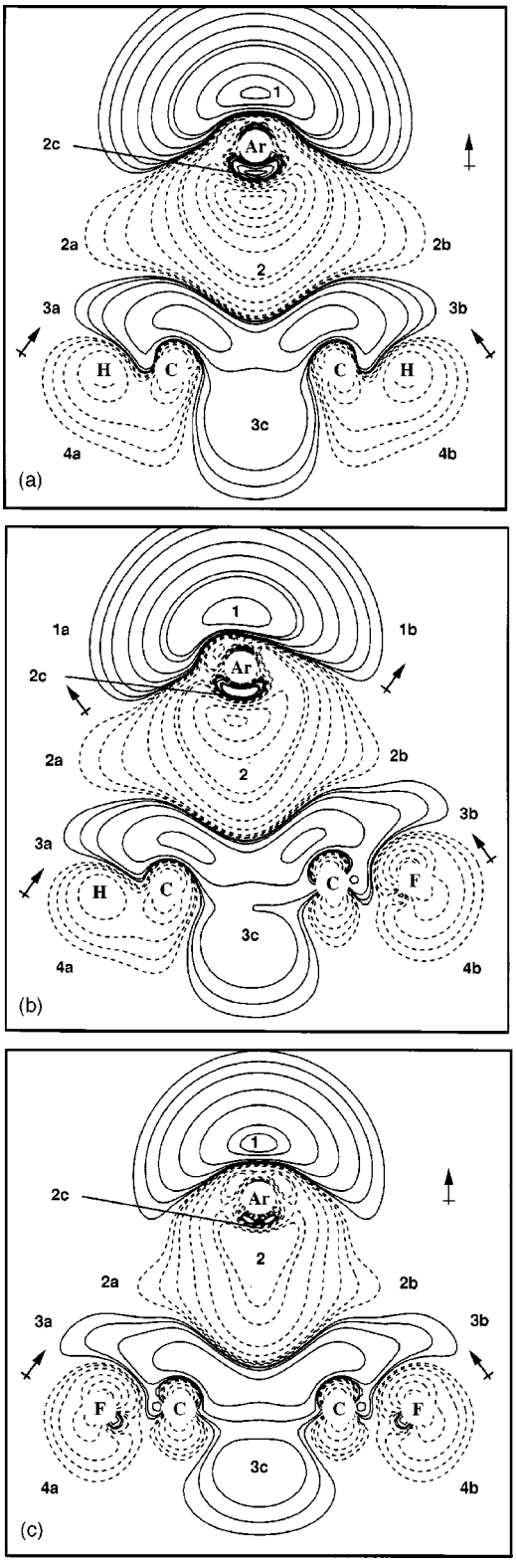

FIG. 4. Contour line diagram of the MP2 difference electron density distribution $\Delta\rho(\mathbf{r})$ [see Eq. (2)] of (a) benzene-argon (BAr), (b) fluorobenzene-argon (FAr), and (c) *p*-difluorobenzene-argon (DAr) calculated with a $[7s4p2d1f/4s3p1d/3s1p]$ basis at optimized geometries. The reference plane is the plane perpendicular to the benzene ring containing Ar and the C–X bonds (X=H or F). Contour lines range from 2×10^{-6} to $2\times10^{-1}[e/\mathrm{Bohr}^3]$. Solid lines correspond to an increase of electron density upon complex formation, dashed lines to a decrease. Regions of increase and decrease of electron density are marked by small numbers. Local induced dipole moments are schematically indicated by arrows where the head of the arrow indicates the negative end of the dipole (chemical notation).

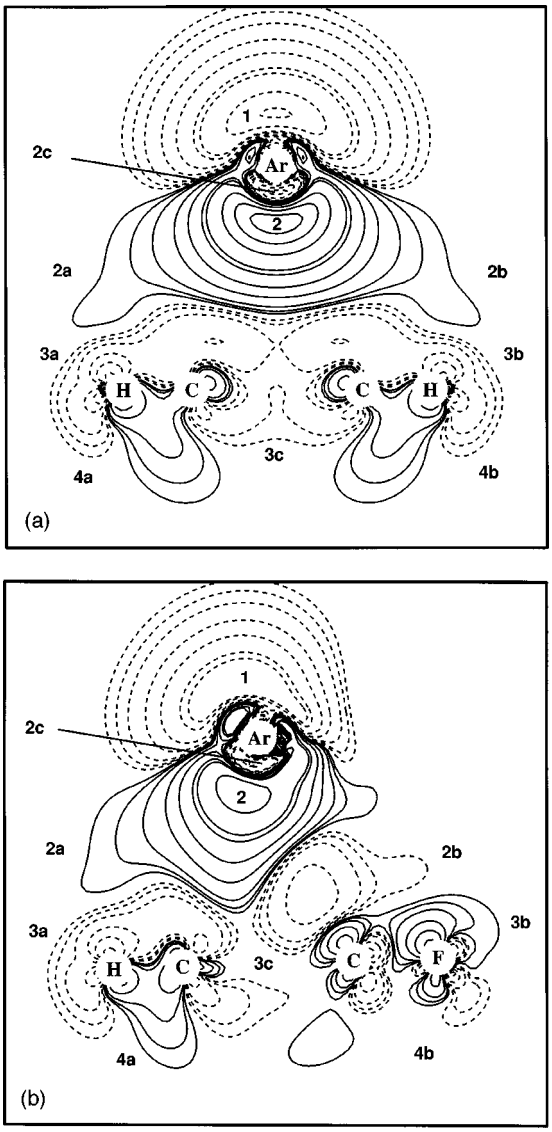

FIG. 5. Contour line diagram of the MP2 difference electron density distribution $\Delta\Delta\rho(\mathbf{r})$ [see Eq. (3)] of (a) DAr-BAr and (b) DAr-FAr calculated with a $[7s4p2d1f/4s3p1d/3s1p]$ basis at optimized geometries. The reference plane is the plane perpendicular to the benzene ring that contains Ar and the C–X bonds (X=H or F). Contour lines range from 2×10^{-6} to $2\times10^{-1}[e/\mathrm{Bohr}^3]$. Solid lines correspond to an increase of electron density upon complex formation, dashed lines to a decrease. Regions of increase and decrease of electron density are marked by small numbers.

Differences between the density distributions of the three complexes are analyzed by calculating the difference density distribution:

$$\Delta\Delta\rho(\mathbf{r}) = \left[\rho(\text{complex } 1) - \sum_i \rho_i(1,\text{monomer}_i^{\text{DCBS}})\right] - \left[\rho(\text{complex } 2) - \sum_j \rho_j(2,\text{monomer}_j^{\text{DCBS}})\right], \tag{3}$$

where 1 and 2 denote complexes BAr, FAr, and DAr and the monomers of a given complex correspond to Ar and one of the three benzenes. For the purpose of determining $\Delta\Delta\rho(\mathbf{r})$, complex 2 is recalculated in the geometry of complex 1

TABLE IV. Polarizabilities of benzene (B), fluorobenzene (F), and difluorobenzene (D) evaluated at the MP2/[7s4p2d1f/4s3p1d/3s1p] level of theory.[a]

Polarizability Å^3	(B)	(F)	(D)
α_π	6.33	6.18	6.04
$\alpha_{\sigma 1}$	11.81	11.88	11.96
$\alpha_{\sigma 2}$	11.81	11.70	11.67
α_{iso}	9.98	9.91	9.89
α_{exp}	10.0	10.3	

[a]The polarizability components are given for the principle axis system, where one axis complies with the π direction and the other two with the in-plane directions.

(apart from the C–X bond lengths with X=H or F). In this way, the differences caused by the replacement of H by F become visible [see Figs. 5(a) and 5(b)]. In DAr, there is more density in the region between the monomers (region 2), which means that exchange-repulsion is smaller for DAr than for BAr (533 versus 507 cm^{-1}, Table II). Accordingly, the polarization of the electron density of the complex partners of DAr is also smaller. There is less density in regions 1 and 2c, more in region 2 [Figure 5(a)], thus decreasing the absolute magnitude of the induction term relative to that of BAr (-177 versus -150 cm^{-1}, Table II).

The decrease in exchange-repulsion calculated for DAr leads also to a decrease in the coupling terms $E^{(2)}_{\text{exch-ind}}$ and $E^{(2)}_{\text{exch-disp}}$ (159 versus 146, 59 versus 55 cm^{-1}, Table II) thus stabilizing complex DAr relative to complex BAr. The tighter binding of the π-density toward the nuclear framework does not only decrease exchange repulsion but also stabilizing dispersion interactions (from -772 to -761 cm^{-1}, Table II). This is due to the fact that tighter binding of the density reduces the π-component of the dipole polarizability (benzene: 6.33; fluorobenzene: 6.18; difluorobenzene: 6.04 Å^3, MP2/[7s4p2d1f/4s3p1d/3s1p], Table IV). Hence, in total the changes in exchange repulsion (see Figs. 4 and 5), which increase the stability of DAr, are compensated by changes in the induction and the dispersion term, which decrease the stability of DAr. Accordingly, complexes BAr and DAr possess the same stability.

Complex FAr takes an intermediate position as to the changes in the various interaction terms [see Fig. 4(b) and Table II] and, therefore, similar considerations as in the case of BAr and DAr apply to explain the fact that the complex stability does not change significantly. The Ar atom is shifted toward the F atom because of the decrease in exchange-repulsion (also, the Ar atom can interact with seven rather than six atoms possessing π-electrons). The shift in the position of Ar leads to some asymmetry in the charge polarization in regions 1, 2, and 3. The charge build up in 1 is shifted slightly from 1b toward 1a. Also, there is more electron density depleted from region 2b than from 2c while the build up of density is somewhat stronger in region 3b than in region 3a.

IV. CONCLUSIONS

A number of conclusions can be drawn from this investigation.

(i) BSSE- and ZPVE-corrected binding energies ΔE_o calculated at the MP2/[7s4p2d1f/4s3p1d/3s1p] level of theory (357, 351, 364 cm^{-1}, Table II) agree reasonably (deviations between 7 and 25 cm^{-1}) with experimental binding energies of 340 (BAr), 344 (FAr), and 339 cm^{-1} (DAr).[13,17–20] We note that the inclusion of BSSE corrections improves binding energies by 80% and more, but at least another 10% improvement is due to ZPVE corrections, which is often overlooked.

(ii) BSSE-corrected complex geometries are in line with experimentally determined geometries. In particular, the MP2/[7s4p2d1f/4s3p1d/3s1p] values of the distance $R_{\pi_{\text{CM}}-\text{Ar}}$ [3.592 (BAr); 3.588 ($R_\perp$ for FAr; $R_\parallel=0.154$); 3.578 Å (DAr)] agree well with the corresponding experimental values of 3.582, 3.572 (0.228), and 3.550 Å.[7,9,10] BSSE-uncorrected geometry optimizations, however, underestimate this parameter by $\sim$0.03 Å.

(iii) The BSSE also has serious consequences for the SAPT analysis of binding energies. The noninclusion of BSSE corrections in the geometry optimizations influences the magnitude and trends of the various interaction energy components. The absolute magnitude of the calculated contributions to the binding energy is exaggerated, which is mainly due to an underestimation of the distance $R_{\pi_{\text{CM}}-\text{Ar}}$.

(iv) The presence of electron-withdrawing substituents such as F in the aromatic ring has a strong effect on the electronic structure of the benzene ring and, by this, on the complex formation. As shown in Fig. 3, the π-density above and below the ring is depleted by contraction toward the C atoms of the ring. This leads to a reduction of exchange repulsion and explains the shorter $R_\perp$ values for FAr (3.588) and DAr (3.578 compared to 3.592 Å for BAr).

(v) The contraction of the π-density caused by F substituents also has consequences for stabilizing induction and dispersion forces. Both are reduced where in the first case the decrease in exchange repulsion decreases also the polarizing power of the benzene monomer. Induced moments at argon become smaller and hence the induction contribution. The decrease of dispersion interactions results from the fact that with a tighter binding of the π-density the π-component of the polarizability becomes smaller (Table IV).

(vi) Both the exchange-repulsion and dispersion energies influence the location of the argon atom in the equilibrium geometries of these complexes, albeit in different ways. Thus the diminished electron density of the fluorobenzene leads to a much closer approach of the argon atom to the fluorine atom in its attempt to maximize the dispersive interactions. Since the smaller intermolecular separation also leads to an increase in the exchange-repulsion terms, the net binding energies are similar for both benzene and the fluorinated benzenes.

(vii) Using results obtained in this work, we can predict that with increasing F substitution the complex stability should not change strongly because there will be a balance between decreasing exchange-repulsion effects and decreasing dispersion interactions. This balance is more pronounced for highly symmetrical complexes. Similar predictions do not hold for other halogen-substituted benzene-argon complexes because in these cases the polarizability increases sig-

nificantly in the series of F-, Cl-, Br-, and I-substituted benzenes, as well as with the number of halogen substituents. This leads to larger dispersion forces accompanied only by a small increase in exchange-repulsion so that the overall complex stability increases.

(viii) In the halogen-substituted benzene-argon complexes, exchange-repulsion and dispersion effects dominate. An adequate description of the latter requires correlation corrected methods. Conventional methods such as HF theory can only be used for predicting complex properties if these are dominated by electrostatic and exchange forces,[63,64] as is the case for conventional hydrogen bonded complexes.

(ix) The SAPT and electron density descriptions, if correctly carried out, after considering BSSE corrections, lead to similar, largely complementary descriptions of the complexes investigated in this work. This supports arguments that the density description can be used (a) for a qualitative rationalization of complex properties such as equilibrium geometry, binding energy, dipole moment, etc., and (b) for the interpretation of SM binding energies and the SAPT decomposition of binding energies.

(x) Analysis of difference electron density distributions reflects, in particular, exchange-repulsion effects by indicating areas with a decrease or an increase of electron density caused by complex formation. The pattern of depletion and concentration regions indicates induced dipole (multipole) moments and can be used to estimate induction forces. Dispersion forces are proportional to the dipole polarizabilities of the monomers, as volume quantities are related to the space filled out by the density of the monomer (as, e.g., given by the 0.001 a.u. contour line of the electron density). By comparing this space with the help of the difference electron density distribution of closely related monomers as those in the current case, the relative polarizabilities and the relative magnitude of dispersion forces can be estimated.

ACKNOWLEDGMENTS

Two of the authors (P.T.) and (K.S.K.) thank MOST/STEPI (CRIP) for financial support. E.K. and D.C. acknowledge support by the Swedish Natural Science Research Council (NFR) and the Nationellt Superdatorcentrum (NSC), Linköping, Sweden. We thank Professor Bernhard Brutschy for helpful discussions on the experimental aspects of the FBz-Ar and DFBz-Ar complexes. We thank Professor Krzysztof Szalewicz for providing us with a copy of SAPT.

[1] P. Hobza, H. L. Selzle, and E. W. Schlag, Chem. Rev. **94**, 1767 (1994).
[2] P. M. Felker, P. M. Maxton, and M. W. Schaeffer, Chem. Rev. **94**, 1787 (1994).
[3] H. J. Neusser and H. Krause, Chem. Rev. **94**, 1829 (1994).
[4] A. van der Avoird, P. E. S. Wormer, and R. Moszynski, Chem. Rev. **94**, 1931 (1994); P. E. S. Wormer and A. van der Avoird, *ibid.* **100**, 4109 (2000).
[5] C. E. H. Dessent and K. Müller-Dethlefs, Chem. Rev. **100**, 3999 (2000).
[6] K. S. Kim, P. Tarakeshwar, and J. Y. Lee, Chem. Rev. **100**, 4145 (2000).
[7] Th. Weber, A. von Bargen, E. Riedle, and H. J. Neusser, J. Chem. Phys. **92**, 90 (1990); Th. Weber, E. Riedle, H. J. Neusser, and E. W. Schlag, Chem. Phys. Lett. **183**, 77 (1991).
[8] M.-C. Su, H.-K. O, and C. S. Parmenter, Chem. Phys. **156**, 261 (1991).
[9] W. Stahl and J.-U. Grabow, Z. Naturforsch. A **47**, 681 (1992).
[10] R. Sussmann, R. Neuhausser, and H. J. Neusser, Can. J. Phys. **72**, 1179 (1994).
[11] R. A. Appleman, S. A. Peebles, and R. L. Kuczkowski, J. Mol. Struct. **446**, 55 (1998).
[12] C. Riehn, A. Weichert, M. Zimmermann, and B. Brutschy, Chem. Phys. Lett. **299**, 103 (1999).
[13] H. Krause and H. J. Neusser, J. Chem. Phys. **99**, 6278 (1993); E. Riedle and A. van der Avoird, *ibid.* **104**, 882 (1996).
[14] Th. L. Grebner, P. v. Unold, and H. J. Neusser, J. Phys. Chem. A **101**, 158 (1997).
[15] R. Neuhauser, J. Braun, H. J. Neusser, and A. van der Avoird, J. Chem. Phys. **108**, 8408 (1998).
[16] R. G. Satink, H. Piest, G. von Helden, and G. Meijer, J. Chem. Phys. **111**, 10750 (1999).
[17] G. Lembach and B. Brutschy, J. Chem. Phys. **107**, 6156 (1997).
[18] G. Lembach and B. Brutschy, J. Phys. Chem. **100**, 19758 (1996).
[19] G. Lembach and B. Brutschy, J. Phys. Chem. A **102**, 6068 (1998).
[20] S. M. Bellm, J. R. Gascooke, and W. D. Lawrance, Chem. Phys. Lett. **330**, 103 (2000).
[21] E. Arunan, T. Emilsson, and H. S. Gutowsky, J. Chem. Phys. **101**, 861 (1994).
[22] Th. Brupbacher, J. Makarewicz, and A. Bauder, J. Chem. Phys. **101**, 9736 (1994).
[23] E. Reidle, R. Sussmann, Th. Weber, and H. J. Neusser, J. Chem. Phys. **104**, 865 (1996).
[24] W. Lu, Y. Hu, and S. Yang, J. Chem. Phys. **108**, 12 (1998).
[25] T. Droz, T. Bürgi, and S. Leutwyler, J. Chem. Phys. **103**, 4035 (1995).
[26] P. Parneix, F. G. Amar, and P. Bréchignac, Chem. Phys. **239**, 121 (1998).
[27] V. Bernshtein and I. Orel, J. Chem. Phys. **112**, 686 (2000).
[28] P. Hobza, H. L. Selzle, and E. W. Schlag, J. Chem. Phys. **95**, 391 (1991).
[29] P. Hobza, O. Bludský, H. L. Selzle, and E. W. Schlag, J. Chem. Phys. **97**, 335 (1992).
[30] P. Hobza, H. L. Selzle, and E. W. Schlag, J. Chem. Phys. **99**, 2809 (1993).
[31] W. Klopper, H. P. Lüthi, Th. Brupbacher, and A. Bauder, J. Chem. Phys. **101**, 9747 (1994).
[32] P. Hobza, O. Bludský, H. L. Selzle, and E. W. Schlag, Chem. Phys. Lett. **250**, 402 (1996).
[33] H. Koch, B. Fernández, and O. Christiansen, J. Chem. Phys. **108**, 2784 (1998).
[34] J. Vacek, P. Hobza, and J. Jortner, J. Phys. Chem. A **102**, 8268 (1998).
[35] H. Koch, F. Fernández, and J. Makarewicz, J. Chem. Phys. **111**, 198 (1999).
[36] I. López-Tocón, J. C. Otero, M. Becucci, G. Pietraperzia, E. Castellucci, Chem. Phys. **249**, 113 (1999).
[37] E. Kraka, D. Cremer, U. Spoerel, I. Merke, W. Stahl, and H. Dreizler, J. Phys. Chem. **99**, 12466 (1995).
[38] U. Spoerel, H. Dreizler, W. Stahl, E. Kraka, and D. Cremer, J. Phys. Chem. **100**, 14298 (1996).
[39] J. J. Oh, I. Park, R. J. Wilson, S. A. Peebles, R. L. Kuczkowski, E. Kraka, and D. Cremer, J. Chem. Phys. **113**, 9051 (2000).
[40] P. Tarakeshwar, K. S. Kim, and B. Brutschy, J. Chem. Phys. **110**, 8501 (1999).
[41] P. Tarakeshwar, H. S. Choi, S. J. Lee, J. Y. Lee, K. S. Kim, T. K. Ha, J. H. Jang, J. G. Lee, and H. Lee, J. Chem. Phys. **111**, 5838 (1999); K. S. Kim, J. Y. Lee, H. S. Choi, J. Kim, and J. H. Jang, Chem. Phys. Lett. **265**, 497 (1997).
[42] P. Tarakeshwar, K. S. Kim, and B. Brutschy, J. Chem. Phys. **112**, 1769 (2000).
[43] M. A. Spackman, J. Phys. Chem. **93**, 7594 (1989).
[44] P. C. Hariharan and J. A. Pople, Chem. Phys. Lett. **16**, 217 (1972).
[45] G. Chalasiński, D. J. Funk, J. Simons, and W. H. Breckenridge, J. Chem. Phys. **87**, 3569 (1987).
[46] G. Chalasiński and M. M. Szczęśniak, Chem. Rev. **94**, 1723 (1994); G. Chalasiński and M. M. Szczęśniak, *ibid.* **100**, 4227 (2000).
[47] B. Jeziorski, R. Moszynski, and K. Szalewicz, Chem. Rev. **94**, 1887 (1994); K. Szalewicz and B. Jeziorski, *Molecular Interactions–From van der Waals to Strongly Bound Complexes*, edited by S. Scheiner (Wiley, New York, 1997), p. 3.
[48] B. Jeziorski, R. Moszynski, A. Ratkiewicz, S. Rybak, K. Szalewicz, and H. L. Williams, in *Methods and Techniques in Computational Chemistry: METECC-94. Vol. B. Medium Size Systems*, edited by E. Clementi (STEF, Cagliari, 1993), p. 79.
[49] T. H. Dunning, J. Chem. Phys. **90**, 1007 (1989); D. E. Woon and T. H. Dunning, *ibid.* **98**, 1358 (1993).
[50] S. F. Boys and F. Bernardi, Mol. Phys. **19**, 553 (1970).
[51] S. Simon, M. Duran, and J. J. Dannenberg, J. Chem. Phys. **105**, 11024

(1996); P. Salvador, S. Simon, M. Duran, and J. J. Dannenberg, *ibid.* **113**, 5666 (2000).
[52] M. J. Frisch, G. W. Trucks, H. B. Schlegel *et al.*, GAUSSIAN 94, Revision A. Gaussian, Inc., Pittsburgh, PA, 1995.
[53] E. Kraka, J. Gräfenstein, Y. He, J. Gauss, F. Reichel, L. Olsson, Z. Konkoli, Z. He, and D. Cremer, COLOGNE2000 (Göteborg University, Göteborg, 2000).
[54] P. Tarakeshwar, H. S. Choi, and K. S. Kim, J. Am. Chem. Soc. **123**, 3323 (2001).
[55] R. Moszyński, B. Jeziorski, A. Ratkiewicz, and S. Rybak, J. Chem. Phys. **99**, 8856 (1993); R. Moszyński, B. Jeziorski, and K. Szalewicz, *ibid.* **100**, 1312 (1994); R. Moszyński, B. Jeziorski, S. Rybak, K. Szalewicz, and H. L. Williams, *ibid.* **100**, 5080 (1994); S. Rybak, B. Jeziorski, and K. Szalewicz, *ibid.* **95**, 6576 (1991); R. Moszyński, S. Cybulski, and G. Chałasiński, *ibid.* **100**, 4998 (1994); G. Chałasiński and B. Jeziorski, Theor. Chim. Acta **46**, 277 (1977); R. Moszyński, T. Korona, P. E. S. Wormer, and A. van der Avoird, J. Phys. Chem. A **101**, 4690 (1997).
[56] K. Szalewicz, S. J. Cole, W. Kolos, and R. J. Bartlett, J. Chem. Phys. **89**, 3662 (1988).
[57] R. Bukowski, K. Szalewicz, and C. Chabalowski, J. Phys. Chem. A **103**, 7322 (1999).
[58] A. Milet, R. Moszyński, P. E. S. Wormer, and A. van der Avoird, J. Phys. Chem. A **103**, 6811 (1999).
[59] P. Tarakeshwar, K. S. Kim, and B. Brutschy, J. Chem. Phys. **114**, 1295 (2001).
[60] P. Hobza, O. Bludský, and S. Suhai, Phys. Chem. Chem. Phys. **1**, 3073 (1999).
[61] Unpublished results.
[62] A. J. Stone, *The Theory of Intermolecular Forces* (Clarendon, Oxford, 1996).
[63] A. D. Buckingham and P. W. Fowler, J. Chem. Phys. **79**, 6426 (1983).
[64] A. C. Legon and D. J. Millen, Faraday Discuss. Chem. Soc. **73**, 71 (1982).